Automatica 110 (2019) 108536

Contents lists available at ScienceDirect

Automatica

journal homepage: www.elsevier.com/locate/automatica

On the synthesis of an integrated active LPV FTC scheme using sliding modes☆

Lejun Chen *, Halim Alwi, Christopher Edwards

College of Engineering, Mathematics and Physics Sciences, University of Exeter, UK

ARTICLE INFO

Article history:
Received 7 December 2017
Received in revised form 3 May 2019
Accepted 26 July 2019
Available online xxxx

Keywords:
Sliding mode observer
Fault tolerant control
Linear parameter-varying

ABSTRACT

This paper proposes an integrated fault tolerant control scheme for a class of systems, modelled in a linear parameter-varying (LPV) framework and subject to sensor faults. The gain in the LPV sliding mode observer (SMO) and the gain in the LPV static feedback controller are synthesized simultaneously to optimize the performance of the closed-loop system in an $\mathcal{L}_2$ sense. In the proposed scheme, the sensor faults are reconstructed by the SMO and these estimates are subsequently used to compensate the corrupted sensor measurements before they are used by the feedback controller. To address the synthesis problem, an iterative algorithm is proposed based on a diagonalization of the closed-loop Lyapunov matrix at each iteration. As a result the NP-hard, non-convex linear parameter-varying bilinear matrix inequality (LPV/BMI) associated with the Bounded Real Lemma formulation, is simplified into a tractable convex LPV/LMI problem. A benchmark scenario, involving the loss of the angle of attack sensor in a civil aircraft, is used as a case study to demonstrate the effectiveness of the scheme.

1. Introduction

In contrast to passive fault tolerant control (FTC) which essentially extends robust control concepts by considering faults as a specific form of uncertainty, active FTC schemes allow the controller to respond to the effects of faults via control reconfiguration (Blanke, Kinnaert, Lunze, & Staroswiecki, 2016; Lan & Patton, 2016). Traditionally, in the design of active FTC schemes, the feedback control component and the associated fault detection and isolation (FDI) scheme are designed independently (Alwi & Edwards, 2008; Blanke et al., 2016; Chen & Patton, 1999; Zhang & Jiang, 2008). Since the FDI performance within closed-loop systems is unavoidably affected by system uncertainty, especially when the fault and system uncertainties occur in the same channel or are in a similar frequency range, there always exists a unidirectional robustness interaction between the control system and FDI scheme (Lan & Patton, 2016). Exploiting increasing computer power and modern optimization techniques, the earliest integrated control and FDI schemes appeared in Kilsgaard, Rank, Niemann, and Stoustrup (1996) and Nett, Jacobson, and Miller (1988) and Niemann and Stoustrup (1997) where the control and FDI objectives were combined together and solved simultaneously to ensure robust control and FDI performance. However, these studies focused on 'integrated FDI/control' without considering active FTC system design (Lan & Patton, 2016). In the literature, the concept of 'integrated FDI/control' (Lan & Patton, 2016) has successfully been applied to linear and nonlinear systems. Many of the existing 'integrated FDI/control' results are based around the 'four-parameter controller' method (Nett et al., 1988; Niemann & Stoustrup, 1997), $\mathcal{H}_\infty$-optimization (Marcos & Balas, 2005a, 2005b; Wang & Yang, 2009; Weng, Patton, & Cui, 2008) and variants thereof, e.g. mixed $\mathcal{H}_2/\mathcal{H}_\infty$ approaches (Khosrowjerdi, Nikoukhah, & Safari-Shad, 2004) and mixed $\mathcal{H}_-/\mathcal{H}_\infty$ methods (Davoodi, Meskin, & Khorasani, 2014; Zhong & Yang, 2015). As argued in Lan and Patton (2016), closed-loop FDI-based FTC systems are affected by both the system uncertainty and the diagnosis uncertainty. This implies that there exist so-called bi-directional robustness interactions between the FDI component and the FTC scheme and it is necessary to consider 'integrated FDI/FTC' via a simultaneous optimization/design procedure (Ding, 2009; Lan & Patton, 2016; Zhang & Jiang, 2006). The 'integrated FDI/FTC' paradigm has proved very successful and has been applied to linear parameter varying (LPV) systems (Rodrigues, Hamdi, Braiek, & Theilliol, 2014), Takagi–Sugeno (T–S) Fuzzy systems (Lan & Patton, 2017a), and nonlinear systems (Gao & Ding, 2007; Jiang, Staroswiecki, & Cocquempot, 2006; Kabore & Wang, 2001; Lan & Patton, 2017b; Yang, Jiang, & Staroswiecki, 2009).

☆ The work in this paper is supported by European Commission, Seventh Framework Programme, FP7 Transport, Grant/Award Number: 314544 (RECONFIGURE). The material in this paper was partially presented at the 54th IEEE Conference on Decision and Control, December 15-18, 2015, Osaka, Japan. This paper was recommended for publication in revised form by Associate Editor Constantino M. Lagoa under the direction of Editor Richard Middleton.

* Corresponding author.
E-mail addresses: Lejun.Chen@exeter.ac.uk (L. Chen), h.alwi@exeter.ac.uk (H. Alwi), c.edwards@exeter.ac.uk (C. Edwards).

https://doi.org/10.1016/j.automatica.2019.108536

The last decades have seen an increase in interest of using sliding mode concepts for both FDI, FTC (Alwi, Edwards, & Tan, 2011) and integrated FDI/FTC (Lan & Patton, 2016). This is particularly true of the use of sliding mode observers (SMOs) for fault estimation (see for example in de Loza, Bejarano, and Fridman (2013), Efimov, Fridman, Raissi, Zolghadri, and Seydou (2012), Levant (1998) and Shtessel, Edwards, Fridman, and Levant (2013)). However, in the literature, only a few papers have developed observers to estimate/reconstruct unknown input signals/faults for LPV systems (Chen, Patton and Goupil, 2016; Ichalal & Mammar, 2015; Kulcsr, Bokor, & Shinar, 2010; Rodrigues et al., 2014). In Kulcsr et al. (2010), an LPV geometric fault estimator was developed, but a parameter-dependent similarity transformation needs to be solved. In terms of designing conventional Luenberger-like LPV observers (Chen, Patton et al., 2016; Rodrigues et al., 2014) or LPV UIOs (Ichalal & Mammar, 2015), for the purpose of satisfying the classical rank conditions to decouple the disturbance from the state estimator error, a full rank output fault distribution matrix is required. Compared with the conventional LPV fault estimation approaches, SMO based approaches provide finite time behaviour and the fault estimates possess strong robustness against unmatched uncertainty.

In this paper, an LPV sliding mode observer and an LPV static feedback controller are synthesized simultaneously to achieve robust fault tolerant control. It is well known that sliding mode observers can be used to generate robust simultaneous state and fault signal estimates despite model uncertainties and external disturbances (Alwi et al., 2011; Edwards, Spurgeon, & Patton, 2000; Shtessel et al., 2013). In this paper, estimates of the sensor faults from the sliding mode observer (SMO) will be used to correct the corrupted sensor measurement signals before they are used by the controller. As a consequence, the controller does not need to be reconfigured to adapt to sensor faults. Employing fault estimation within an active FTC scheme reduces the design complexity and considers bi-directional uncertainty. In this paper, a static feedback control law and a SMO for fault estimation are employed. This leads to the problem of simultaneous synthesis of the gain matrices for both the sliding mode observer and the static feedback controller. Using the Bounded Real Lemma (BRL), the formulation becomes as an LPV/BMI optimization problem which is NP-hard and non-convex (Blondel & Tsitsiklis, 1997). To address this issue, a novel iterative LMI based algorithm is developed to transform the LPV/BMI problem into a tractable and convex LPV/LMI problem, and monotonic convergence to a (local) optimum is ensured. This paper extends the ideas originally proposed in Chen, Alwi and Edwards (2015). Compared with Chen, Alwi et al. (2015), in this paper, the development has been restructured, and the theory has undergone significant changes and expansion to accommodate a wider more general class of uncertainty. Furthermore, the scheme has been validated using a high-fidelity nonlinear aircraft benchmark model.

This paper is organized as follows: in Section 2, the sliding mode based integrated active sensor FTC problem is formulated. In Section 3, the synthesis method is introduced to deal with the integrated design problem. Finally, a high-fidelity commercial aircraft benchmark problem is described in Section 4 to demonstrate the effectiveness of the scheme. The notation used in this paper is reasonably standard. In particular $\mathbb{R}$ represents the field of real numbers and $\mathbb{R}^{n\times m}$ denotes matrices with n rows and m columns. The symbol $\mathbb{S}_n^+$ will be used to represent symmetric positive definite matrices of order n.

2. Preliminary

Consider the uncertain LPV system subject to sensor faults

$$\begin{aligned}\dot{x}_p(t) &= A_p(\rho)x_p(t) + B_p(\rho)u_p(t) + M_p(\rho)\xi(y_p,t)\\ y_p(t) &= C_{p,1}x_p(t) + H_p f(t)\\ z_\infty(t) &= C_{p,2}x_p(t)\end{aligned} \tag{1}$$

In (1), the system matrix $A_p(\rho)\in\mathbb{R}^{n\times n}$, and the input distribution matrix $B_p(\rho)\in\mathbb{R}^{n\times m}$. The two output distribution matrices $C_{p,1}\in\mathbb{R}^{p\times n}$, $C_{p,2}\in\mathbb{R}^{h\times n}$ are fixed and do not depend on the scheduling parameter ρ. The matrix $M_p(\rho)\in\mathbb{R}^{n\times l}$ is the uncertainty distribution matrix and the fixed matrix $H_p\in\mathbb{R}^{p\times q}$ represents the sensor fault distribution matrix and it is assumed $q<p$. Furthermore, the columns of H_p are assumed to belong to the standard basis for $\mathbb{R}^p$. In (1) it is assumed that the signals $u_p(t)$ and $y_p(t)$ are measurable. Suppose in fact that $y_p(t)$ represents the measured state $x_p(t)$, potentially corrupted by the faults $f(t)$. As in Zhou and Doyle (1998), $z_\infty(t)$ denotes the performance signal which is to be kept small by means of feedback control. In (1), the fault signals $f(t)$ are unknown but are assumed to be subject to $\|f(t)\|\le\beta$, where $\beta>0$ is a known scalar. Finally, the signal $\xi(y_p,t)$ denotes lumped system uncertainty which is assumed to be bounded by $\|\xi(t)\|\le c_1\|y_p(t)\|+c_2(t)$ where c_1 is a known positive scalar and the function $c_2(t)$ is unknown but is subject to $\|c_2(t)\|\le d$.

Assumption 2.1. The (known) scheduling parameter $\rho(t)$ associated with the plant is smooth and slowly varying.

Remark 2.1. Assumption 2.1 is a common assumption in LPV papers (see for example in Bokor and Balas (2004), Hecker and Pififer (2014) and Szaszi, Marcos, Balas, and Bokor (2005)) and is quite reasonable for a large class of real engineering systems — for example the civil aircraft example discussed later in the paper. When the scheduling parameter is potentially fast-varying, the rate of change of the scheduling parameter will influence the robust stability and performance of the system (Pfifer & Seiler, 2015; Shamma, 2012; Wu, 1996). In this situation a more generic design framework involving parameter-dependent Lyapunov functions needs to be considered (e.g. see Chen, Edwards, and Alwi (2017) for the development of an LPV SMO).

Remark 2.2. In this paper, the scheduling parameter $\rho(t)$ is assumed to be perfectly measured. Work where $\rho(t)$ is unknown or uncertain appears for example in Chandra, Alwi, and Edwards (2017), Chen, Edwards and Alwi (2015) and Sato and Peaucelle (2013).

Assumption 2.2. The LPV matrices $A_p(\rho)$, $B_p(\rho)$ and $M_p(\rho)$ belong to a polytope Ω, and they can be written as

$$\begin{aligned}A_p(\rho) &= \sum_{i=1}^{n_\rho}\zeta_i(\rho)A_i \quad B_p(\rho) = \sum_{i=1}^{n_\rho}\zeta_i(\rho)B_i\\ M_p(\rho) &= \sum_{i=1}^{n_\rho}\zeta_i(\rho)M_i\end{aligned} \tag{2}$$

where $\zeta_i(\rho)\ge 0$ satisfy $\sum_{i=1}^{n_\rho}\zeta_i(\rho)=1$, and the matrices $A_i\in\mathbb{R}^{n\times n}$, $B_i\in\mathbb{R}^{n\times m}$ and $M_i\in\mathbb{R}^{n\times l}$ are known.

The objective is to develop a feedback control scheme for (1) to keep the performance signal $z_\infty(t)$ small, which is tolerant to the measurement faults $f(t)$ affecting $y_p(t)$. The idea is to develop an observer scheme to estimate $f(t)$ and then use the estimate to compensate the fault in the feedback loop. In this context, there are links with other areas of research e.g. 'disturbance compensation' (Chen, Yang, Guo and Li, 2016).

In this paper, the goal is to achieve *an integrated synthesis of both the fault estimator and the controller* meaning the controller and observer gains are designed simultaneously rather than independently. The scheme is assumed to have the FTC architecture as shown in Fig. 1. In Fig. 1, there are two elements to be synthesized: the scheduled static feedback gain

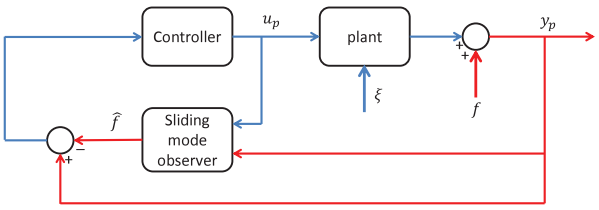

Fig. 1. Schematic of integrated active FTC.

$K(\rho)$; and the gains associated with the sliding mode observer. This framework has been considered in earlier papers (Alwi, Edwards, & Marcos, 2012) but previously the controller and observer were designed independently whereas here they will be designed simultaneously to optimize an overall performance criterion.

2.1. Controller structure

To simplify the controller design, a pre-filter is introduced before the system inputs in (1): specifically

$$\begin{aligned} \dot{x}_u &= A_u(\rho)x_u + B_u u \\ u_p &= C_u x_u \end{aligned} \tag{3}$$

where $A_u(\rho) \in \mathbb{R}^{m\times m}$, $B_u \in \mathbb{R}^{m\times m}$ with $A_u(\rho)$ quadratically stable for all $\rho \in \Omega$ and $\det(B_u) \neq 0$. Then, with respect to the (virtual) input u, the augmented system is

$$\begin{aligned} \begin{bmatrix} \dot{x}_p \\ \dot{x}_u \end{bmatrix} &= \underbrace{\begin{bmatrix} A_p(\rho) & B_p(\rho)C_u \\ 0 & A_u(\rho) \end{bmatrix}}_{A_c(\rho)} \underbrace{\begin{bmatrix} x_p \\ x_u \end{bmatrix}}_{x_c} + \underbrace{\begin{bmatrix} 0 \\ B_u \end{bmatrix}}_{B_c} u + \underbrace{\begin{bmatrix} M_p(\rho) \\ 0 \end{bmatrix}}_{M_c(\rho)} \xi \\ y_p &= \underbrace{\begin{bmatrix} C_{p,1} & 0_{p\times m} \end{bmatrix}}_{C_c} \begin{bmatrix} x_p \\ x_u \end{bmatrix} + H_p f(t) \\ z_\infty &= \underbrace{\begin{bmatrix} C_{p,2} & 0_{h\times m} \end{bmatrix}}_{C_\infty} \begin{bmatrix} x_p \\ x_u \end{bmatrix} \end{aligned} \tag{4}$$

Remark 2.3. The use of a pre-filter results in an augmented system in which the input distribution matrix B_c is fixed. This allows the controller to be synthesized in a more straightforward manner without requiring an infinite number of LMIs. During the design process, a sensible pragmatic choice of pre-filter is one that mimics/relates to the actuator dynamics.

The question of how to achieve appropriate closed loop performance by minimization of the controlled variable z_∞ in (4), by manipulation of u, will now be addressed. Specifically a feedback controller based on y_p will be formulated.

Let $e_f = \hat{f} - f$, then the corrected system measurements

$$\bar{y} := y_p - H_p\hat{f} = C_c x_c - H_p(\hat{f} - f) = C_c x_c - H_p e_f \tag{5}$$

In what follows the proposed feedback control law is given by

$$u = K(\rho)\bar{y} \tag{6}$$

where $K(\rho) \in \mathbb{R}^{m\times p}$ is to be designed and is assumed to have the form $\sum_{i=1}^{n_\rho} \zeta_i(\rho)K_i$.

2.2. Observer structure

To create the fault estimate $\hat{f}$, an LPV sliding mode observer will be proposed. Since by assumption the matrix H_p from (1) is composed of columns from the standard basis of $\mathbb{R}^p$, by reordering the components of y_p, the representation

$$\begin{bmatrix} y_{p,1}(t) \\ y_{p,2}(t) \end{bmatrix} = \begin{bmatrix} C_1 \\ C_2 \end{bmatrix} x_p(t) + \begin{bmatrix} 0 \\ I_q \end{bmatrix} f(t) \tag{7}$$

can be obtained without loss of generality. In (7), $C_1 \in \mathbb{R}^{(p-q)\times n}$, $C_2 \in \mathbb{R}^{q\times n}$ and the signal $y_{p,2}(t)$ denotes the subset of the outputs potentially corrupted by sensor faults, while $y_{p,1}$ are considered fault free. In order to transform this sensor fault problem into a representation more amenable to using sliding mode observers, as in Alwi et al. (2011), define a (stable) filter in the form of

$$\dot{z}_f(t) = -A_f z_f(t) + A_f y_{p,2}(t) \tag{8}$$

where $z_f(t) \in \mathbb{R}^q$ and A_f is a Hurwitz matrix. Note that Eq. (8) represents a coupled first order low pass filter with unit DC gain. Combining (1), (7) and (8), the augmented system can be written as

$$\begin{aligned} \begin{bmatrix} \dot{x}_p(t) \\ \dot{z}_f(t) \end{bmatrix} &= \begin{bmatrix} A_p(\rho) & 0 \\ A_f C_2 & -A_f \end{bmatrix} \begin{bmatrix} x_p(t) \\ z_f(t) \end{bmatrix} + \begin{bmatrix} B_p(\rho) \\ 0 \end{bmatrix} u_p(t) \\ &\quad + \begin{bmatrix} 0 \\ A_f \end{bmatrix} f(t) + \begin{bmatrix} M_p(\rho) \\ 0 \end{bmatrix} \xi(\cdot) \\ \begin{bmatrix} y_{p,1}(t) \\ z_f(t) \end{bmatrix} &= \begin{bmatrix} C_1 & 0 \\ 0 & I_q \end{bmatrix} \begin{bmatrix} x_p(t) \\ z_f(t) \end{bmatrix} \end{aligned} \tag{9}$$

where the newly created partially filtered output signal

$$y := \mathrm{col}(y_{p,1}, z_f) \tag{10}$$

Define a coordinate transformation matrix

$$T_a = \begin{bmatrix} T_s & 0 \\ 0 & I_q \end{bmatrix} \tag{11}$$

where $T_s \in \mathbb{R}^{n\times n}$ is any nonsingular matrix with the property $C_1 T_s^{-1} = \begin{bmatrix} 0 & I_{p-q} \end{bmatrix}$. Such a matrix is guaranteed to exist. Then, applying the coordinate transformation $T_a : (x_p, z_f) \mapsto x_a$ yields the representation

$$\begin{aligned} \underbrace{\begin{bmatrix} \dot{x}(t) \\ \dot{z}_f(t) \end{bmatrix}}_{\dot{x}_a(t)} &= \underbrace{\begin{bmatrix} T_s A_p(\rho) T_s^{-1} & 0 \\ A_f C_2 T_s^{-1} & -A_f \end{bmatrix}}_{A(\rho)} \underbrace{\begin{bmatrix} x(t) \\ z_f(t) \end{bmatrix}}_{x_a(t)} + \underbrace{\begin{bmatrix} T_s B(\rho) \\ 0 \end{bmatrix}}_{B(\rho)} u_p(t) \\ &\quad + \underbrace{\begin{bmatrix} 0 \\ A_f \end{bmatrix}}_{D} f(t) + \underbrace{\begin{bmatrix} T_s M_p(\rho) \\ 0 \end{bmatrix}}_{M(\rho)} \xi(\cdot) \end{aligned} \tag{12}$$

In the new coordinates, the (known) output signal defined in (10) is given by

$$y = C x_a \tag{13}$$

where

$$C = \begin{bmatrix} 0 & I_p \end{bmatrix} \tag{14}$$

Note from (9) that this set of outputs is not directly affected by the additive measurement faults, although the evolution of $(x(t), z_f(t))$ is affected by $f(t)$ (according to (12)). A sliding mode observer will now be developed for the system (12)–(13) based on knowledge of y and u_p.

As in Alwi et al. (2011), consider the dynamical system

$$\dot{z}(t) = A(\rho)z(t) + B(\rho)u_p(t) + G_l(\rho)e_y(t) + G_n\nu(t) \tag{15}$$

where the output estimation error

$$e_y(t) = C(z(t) - x_a(t)) \tag{16}$$

and the *discontinuous* output error injection signal

$$\nu = \begin{cases} -k(t)\dfrac{e_y}{\|e_y\|} & \text{if } e_y \neq 0 \\ 0 & \text{otherwise} \end{cases} \tag{17}$$

In (17), the modulation gain $k(t)$ is a positive design function which will be discussed in the sequel. The observer gain matrix $G_n \in \mathbb{R}^{(n+q)\times p}$, which partially represents the design freedom in (15), is assumed to have the structure

$$G_n = \begin{bmatrix} -L \\ I_p \end{bmatrix} \tag{18}$$

where in turn $L \in \mathbb{R}^{(n+q-p)\times p}$ has the form

$$L = \begin{bmatrix} L_1 & 0 \end{bmatrix} \tag{19}$$

where $L_1 \in \mathbb{R}^{(n+q-p)\times(p-q)}$. In (18) and (19) the gain L_1 constitutes the design freedom to be (optimally) selected.

Define the estimation error $e = z - x_a = \text{col}(e_1, e_y)$, where $e_1 \in \mathbb{R}^{n+q-p}$, then (e_1, e_y) evolves according to

$$\begin{aligned} \begin{bmatrix} \dot{e}_1 \\ \dot{e}_y \end{bmatrix} &= \begin{bmatrix} A_{11}(\rho) & A_{12}(\rho) \\ A_{21}(\rho) & A_{22}(\rho) \end{bmatrix} \begin{bmatrix} e_1 \\ e_y \end{bmatrix} - \begin{bmatrix} 0 \\ D_2 \end{bmatrix} f - \begin{bmatrix} M_1(\rho) \\ M_2(\rho) \end{bmatrix} \xi \\ &\quad + \begin{bmatrix} G_{l1}(\rho) \\ G_{l2}(\rho) \end{bmatrix} e_y + \begin{bmatrix} -L \\ I_p \end{bmatrix} \nu \end{aligned} \tag{20}$$

where the system matrix $A(\rho)$ from (12) has been decomposed into four LPV matrix sub-blocks shown in (20) where in particular $A_{11}(\rho) \in \mathbb{R}^{(n+q-p)\times(n+q-p)}$. Furthermore in (20) it can be easily verified the matrices $D_2 \in \mathbb{R}^{p\times q}$ and $M_2(\rho) \in \mathbb{R}^{p\times q}$ have the specific structure

$$D_2 = \begin{bmatrix} 0 \\ A_f \end{bmatrix} \quad M_2(\rho) = \begin{bmatrix} M_{21}(\rho) \\ 0 \end{bmatrix} \tag{21}$$

where $M_{21}(\rho) \in \mathbb{R}^{(p-q)\times q}$.

Remark 2.4. The special structures inherent in D_2 and $M_2(\rho)$ arise from the augmentation undertaken in (9).

Define a further coordinate transformation depending on the design freedom in (18) according to $e \mapsto T_L e = \tilde{e}$ where

$$T_L = \begin{bmatrix} I_{n+q-p} & L \\ 0 & I_p \end{bmatrix} \tag{22}$$

As a result of this transformation, the system in (20) in the new coordinates $\tilde{e} = col(\tilde{e}_1, e_y)$ can be written

$$\begin{aligned} \underbrace{\begin{bmatrix} \dot{\tilde{e}}_1 \\ \dot{e}_y \end{bmatrix}}_{\dot{\tilde{e}}} &= \begin{bmatrix} \tilde{A}_{11}(\rho) & \tilde{A}_{12}(\rho) \\ \tilde{A}_{21}(\rho) & \tilde{A}_{22}(\rho) \end{bmatrix} \underbrace{\begin{bmatrix} \tilde{e}_1 \\ e_y \end{bmatrix}}_{\tilde{e}} - \begin{bmatrix} 0 \\ D_2 \end{bmatrix} f \\ &\quad - \underbrace{\begin{bmatrix} M_1(\rho) + LM_2(\rho) \\ M_2(\rho) \end{bmatrix}}_{\tilde{M}(\rho)} \xi + \begin{bmatrix} \tilde{G}_{l1}(\rho) \\ \tilde{G}_{l2}(\rho) \end{bmatrix} e_y + \begin{bmatrix} 0 \\ I_p \end{bmatrix} \nu \end{aligned} \tag{23}$$

where in (23) the LPV matrix sub-block $\tilde{A}_{11}(\rho) = A_{11}(\rho) + LA_{21}(\rho)$, and the estimation error $\tilde{e}_1 = e_1 + Le_y$.

Remark 2.5. The structure of the fault distribution matrix associated with f takes the specific form shown in (23) because $LD_2 = 0$ from the special forms of L and D_2 in (20) and (21) respectively.

Remark 2.6. In particular note that the sub-block

$$\tilde{A}_{21}(\rho) = \begin{bmatrix} A_{211}(\rho) \\ A_{212} \end{bmatrix} \tag{24}$$

where $A_{212} \in \mathbb{R}^{q\times(n-p+q)}$ does not depend on the scheduling parameter. This follows because the lower left sub-block of $A(\rho)$ in (15) is independent of the scheduling parameter. This property is preserved despite the sequence of transformations used to establish (23). This structure is exploited in the sequel.

In the error system coordinates in (23) define

$$\begin{bmatrix} \tilde{G}_{l1}(\rho) \\ \tilde{G}_{l2}(\rho) \end{bmatrix} = \begin{bmatrix} -\tilde{A}_{12}(\rho) \\ -\tilde{A}_{22}(\rho) - k_2 I_p \end{bmatrix} \tag{25}$$

where k_2 is a positive design scalar. The following result pertains to the existence of a sliding motion and establishes conditions on the modulation gain k in (17).

Substituting (25) into (23) yields

$$\dot{\tilde{e}} = \tilde{A}_e(\rho)\tilde{e} - \begin{bmatrix} 0 \\ D_2 \end{bmatrix} f - \tilde{M}(\rho)\xi + \begin{bmatrix} 0 \\ I_p \end{bmatrix} \nu \tag{26}$$

where

$$\tilde{A}_e(\rho) = \begin{bmatrix} \tilde{A}_{11}(\rho) & 0 \\ \tilde{A}_{21}(\rho) & -k_2 I_p \end{bmatrix} \tag{27}$$

Suppose there exists a strictly positive definite matrix $P_1 \in \mathbb{R}^{(n+q-p)\times(n+q-p)}$ such that

$$P_1\tilde{A}_{11}(\rho) + \tilde{A}_{11}(\rho)^T P_1 < 0 \tag{28}$$

Then for any positive scalar gain k_2, there exists a positive scalar $p_2 > 0$ such that the matrix $P = \text{diag}(P_1, p_2 I_p)$ satisfies

$$Q(\rho) = P\tilde{A}_e(\rho) + \tilde{A}_e(\rho)^T P < 0 \tag{29}$$

By direct substitution

$$Q(\rho) = \begin{bmatrix} P_1\tilde{A}_{11}(\rho) + \tilde{A}_{11}(\rho)^T P_1 & p_2\tilde{A}_{21}(\rho)^T \\ p_2\tilde{A}_{21}(\rho) & -2p_2 k_2 I_p \end{bmatrix} \tag{30}$$

Using the Schur Complement it can be shown[1] that $Q(\rho) < 0$ if

$$p_2 < -2k_2\lambda_{max}(P_1\tilde{A}_{11}(\rho) + \tilde{A}_{11}(\rho)^T P_1)(\|\tilde{A}_{21}(\rho)\|^2)^{-1} \tag{31}$$

By design assume that $\tilde{A}_{11}(\rho)$, P_1 and k_2 have been chosen so that in (29) the symmetric negative definite matrix

$$Q(\rho) < -Q_0 < 0 \tag{32}$$

where Q_0 is a fixed design matrix. By assumption

$$\|\xi\| \leq c_1\|y_p\| + d := \eta_1(y_p, d) \tag{33}$$

where $\eta_1(\cdot)$ is a known function and d is a known scalar.

Note that (28) and (29) can be evaluated at all vertices of the polytope. Also by construction

$$\tilde{e}^T P \begin{bmatrix} 0 \\ I_p \end{bmatrix} \nu = -kp_2\|e_y\| \tag{34}$$

The objective is to obtain an upper bound on the evolution of $\|\tilde{e}(t)\|$ (to employ as part of the choice of the modulation gain $k(t)$ used to induce sliding). Using the Lyapunov function $V(\tilde{e}) = \tilde{e}^T P\tilde{e}$, if the modulation gain in (17) satisfies $k(t) > \|D_2 f\|$ (which can always be ensured) then from (26)

$$\dot{V} \leq \tilde{e}^T Q(\rho)\tilde{e} - 2\tilde{e}^T P\tilde{M}(\rho)\xi \tag{35}$$

It follows from (35) that

$$\begin{aligned} \dot{V} &\leq -(P^{\frac{1}{2}}\tilde{e})^T P^{-\frac{1}{2}} Q_0 P^{-\frac{1}{2}} P^{\frac{1}{2}}\tilde{e} - 2(P^{\frac{1}{2}}\tilde{e})^T P^{\frac{1}{2}}\tilde{M}(\rho)\xi \\ &\leq -\lambda_{min}(P^{-\frac{1}{2}} Q_0 P^{-\frac{1}{2}})V + 2\sqrt{V}\|P^{\frac{1}{2}}\tilde{M}(\rho)\|\|\xi\| \end{aligned} \tag{36}$$

[1] Assuming $\tilde{A}_{21}(\rho) \neq 0$ the bound in (31) is well defined. If $\tilde{A}_{21}(\rho) = 0$ then $Q(\rho) < 0$ follows trivially for any $p_2, k_2 > 0$ if (28) holds.

where Q_0 is defined in (32) and $\lambda_{min}(\cdot)$ denotes the minimum eigenvalue. Since P is s.p.d., $P^{\frac{1}{2}}$ is well defined. For use in (36) an upper bound on $\|\xi\|$ from (33), depending on $\eta_1(y_p, d)$, is available. Writing $\mathcal{V} = \sqrt{V}$ it follows from (36) that

$$2\mathcal{V}\dot{\mathcal{V}} \leq -\lambda_{min}(P^{-\frac{1}{2}}Q_0P^{-\frac{1}{2}})\mathcal{V}^2 + 2\mathcal{V}\|P^{\frac{1}{2}}\tilde{M}(\rho)\|\eta_1(y_p, d) \tag{37}$$

or equivalently for $\tilde{e} \neq 0$

$$\dot{\mathcal{V}} \leq -q_0\mathcal{V} + \|P^{\frac{1}{2}}\tilde{M}(\rho)\|\eta_1(y_p, d) \tag{38}$$

where the scalar

$$q_0 = \frac{1}{2}\lambda_{min}(P^{-\frac{1}{2}}Q_0P^{-\frac{1}{2}}) > 0 \tag{39}$$

Define the function $\chi(t)$ to be the solution of

$$\dot{\chi}(t) = -q_0\chi(t) + \|P^{\frac{1}{2}}\tilde{M}(\rho)\|\eta_1(y_p, d) \tag{40}$$

where $\chi(0) = 0$. Comparing the solution of (40) with (38) it follows

$$\begin{aligned}\mathcal{V}(t) &\leq e^{-q_0t}\mathcal{V}(0) + \int_0^t e^{-q_0(t-s)}\|P^{\frac{1}{2}}\tilde{M}(\rho)\|\eta_1(y_p, d)ds \\ &= e^{-q_0t}\mathcal{V}(0) + \chi(t)\end{aligned} \tag{41}$$

Let χ_0 be a positive design scalar, then $\chi(t)+\chi_0 > \mathcal{V}(t)$ for $t \geq t_0$ where $t_0 = \min\{0, \frac{1}{q_0}\log(\mathcal{V}(0)/\chi_0)\}$. Define

$$\tilde{\chi}(t) := (\chi(t) + \chi_0)/\sqrt{\lambda_{min}(P)} \tag{42}$$

then since $\mathcal{V} > \sqrt{\lambda_{min}(P)}\|\tilde{e}(t)\|$, by construction $\tilde{\chi}(t) \geq \|\tilde{e}(t)\|$ for $t \geq t_0$.

Remark 2.7. $\tilde{\chi}(t)$ is an available quantity (since $\chi(t)$ can be obtained from solving (40) where $\eta_1(y_p, d)$ is known) and represents an upper bound on $\|\tilde{e}(t)\|$ for all $t > t_0$. This signal will be used in the design of the modulation gain $k(t)$ in (17).

Lemma 2.1. *Consider the case where $t > t_0$ and define*

$$a_{21}(t) = \|\tilde{A}_{21}(\rho)\|; \quad m_2(t) = \|M_2(\rho)\| \tag{43}$$

Then provided the modulation gain $k(t)$ is chosen as

$$k(t) = a_{21}(t)\tilde{\chi}(t) + \|D_2\|\beta + m_2(t)\eta_1(t) + \eta \tag{44}$$

where η is a positive scalar, a sliding motion on

$$\mathcal{S} = \{\tilde{e}(t) \in \mathbb{R}^{n+q} : C\tilde{e}(t) = 0\} \tag{45}$$

can be enforced in finite time.

Proof. Since by assumption $t \geq t_0$, by construction $\|\tilde{e}(t)\| < \tilde{\chi}(t)$, and it follows from (26) that

$$\begin{aligned}e_y^T\dot{e}_y &= e_y^T(\tilde{A}_{21}(\rho)\tilde{e}_1 - k_2e_y - D_2f - M_2(\rho)\xi + \nu) \\ &\leq \|e_y\|(a_{21}(t)\tilde{\chi}(t) + \|D_2\|\beta + m_2(t)\eta_1(t) - k(t)) \\ &\leq -\eta\|e_y(t)\|\end{aligned} \tag{46}$$

if $k(t)$ is chosen as in (44). This ensures sliding takes place in finite time and is maintained in the face of faults (Utkin, 1992). □

During sliding on $\mathcal{S}$, $\dot{e}_y(t) = e_y(t) = 0$, and, as a result of the dynamical collapse, Eq. (23) becomes

$$\begin{aligned}\dot{\tilde{e}}_1 &= \tilde{A}_{11}(\rho)\tilde{e}_1 - (M_1(\rho) + LM_2(\rho))\xi \\ 0 &= \tilde{A}_{21}(\rho)\tilde{e}_1 - D_2f - M_2(\rho)\xi + \nu_{eq}\end{aligned} \tag{47}$$

where ν_{eq} is the equivalent output error injection signal necessary to maintain sliding (Utkin, 1992).

Consider as a potential estimate of the fault

$$\hat{f} = W\nu_{eq} \tag{48}$$

where

$$W = \begin{bmatrix}0 & A_f^{-1}\end{bmatrix} \tag{49}$$

and A_f is the system matrix associated with the filter in (8).

Remark 2.8. The choice of W in (49) is specific to this paper and simplifies the subsequent analysis. However, compared to Alwi et al. (2011), it does introduce an element of conservatism into the results because of the fixed structure of (49).

It follows from (47) and (48) that the fault estimation error

$$e_f = \hat{f} - f = -W\tilde{A}_{21}(\rho)\tilde{e}_1 + WD_2f + WM_2(\rho)\xi - f \tag{50}$$

Then, by choice of W in (49), $WD_2 = I$, $WM_2(\rho) = 0$ and $W\tilde{A}_{21}(\rho) = A_f^{-1}A_{212}$. Consequently the sliding motion error dynamics and the fault estimation error satisfy

$$\begin{aligned}\dot{\tilde{e}}_1 &= \tilde{A}_{11}(\rho)\tilde{e}_1 - (M_1(\rho) + LM_2(\rho))\xi \\ e_f &= -A_f^{-1}A_{212}\tilde{e}_1\end{aligned} \tag{51}$$

Remark 2.9. Note that from (51) in the absence of uncertainty (where $\xi = 0$), $\tilde{e}_1 \to 0$ asymptotically and hence $e_f \to 0$ as $t \to \infty$. However in the presence of uncertainty, generically, $e_f \nrightarrow 0$.

3. Integrated synthesis of the controller and fault estimator

In this section, a control law of the form $u = K(\rho)\bar{y}$ will be synthesized where $\bar{y}$ is the 'corrected' faulty measurement. From (5) and (51)

$$\bar{y} = C_cx_c - C_0\tilde{e}_1 \tag{52}$$

where $C_0 = -H_pA_f^{-1}A_{212}$. Then using (4), (5) and (6)

$$\begin{aligned}\dot{x}_c &= A_c(\rho)x_c + B_cK(\rho)\bar{y} + M_c(\rho)\xi \\ &= (A_c(\rho) + B_cK(\rho)C_c)x_c - B_cK(\rho)C_0\tilde{e}_1 + M_c(\rho)\xi\end{aligned} \tag{53}$$

Suppose the gain $K(\rho)$ in (6) is decomposed as

$$K(\rho) = K_0(\rho) + \Delta(\rho) \tag{54}$$

where $K_0(\rho)$ and $\Delta(\rho)$ have the forms

$$K_0(\rho) = \sum_{i=1}^{n_\rho}\zeta_i(\rho)K_{0i} \quad \Delta(\rho) = \sum_{i=1}^{n_\rho}\zeta_i(\rho)\Delta_i \tag{55}$$

where the matrix $K_0(\rho)$ denotes the initial value of the feedback gain which (at worst) ensures quadratic stability of $(A_c(\rho) + B_cK_0(\rho)C_c)$. The gain $K_0(\rho)$ in (54) can be designed using the plant representation in (1), based on the assumption that the system is fault free (i.e. $f(t) \equiv 0$). Many of the techniques described in Mohammadpour and Scherer (2012) or Rotondo, Nejjari, and Puig (2014) can be exploited to ensure that $(A_c(\rho)+B_cK_0(\rho)C_c)$ is quadratically stable and the closed loop signal $z_\infty(t)$ is kept small in the presence of the uncertainty $\xi(\cdot)$. The matrix $\Delta(\rho)$ is to be determined/designed to improve the performance of the system in the face of faults and to account for the effect of the observer dynamics. Therefore in what follows the components Δ_i which comprise $\Delta(\rho)$ are the decision matrices to be calculated.

To capture the change in performance when $\Delta(\rho) \neq 0$, an error system is defined as

$$\dot{e}_z = (A_c(\rho) + B_cK_0(\rho)C_c)e_z + B_c\Delta(\rho)C_cx_c \tag{56}$$

Eq. (56) represents the difference between the outputs of two systems: one with system matrix $A_c(\rho)+B_cK_0(\rho)C_c$ and one with system matrix $A_c(\rho) + B_c(K_0(\rho) + \Delta(\rho))C_c$.

$$\underbrace{\begin{bmatrix}\dot{e}_z\\ \dot{x}_c\\ \dot{\tilde{e}}_1\end{bmatrix}}_{\dot{x}} = \underbrace{\begin{bmatrix}A_0(\rho) & B_c\Delta(\rho)C_c & 0\\ 0 & A_0(\rho)+B_c\Delta(\rho)C_c & -B_c(K_0(\rho)+\Delta(\rho))C_0\\ 0 & 0 & A_{11}(\rho)+LA_{21}(\rho)\end{bmatrix}}_{A_a(\rho)}\underbrace{\begin{bmatrix}e_z\\ x_c\\ \tilde{e}_1\end{bmatrix}}_{x} + \underbrace{\begin{bmatrix}0\\ M_c(\rho)\\ -(M_1(\rho)+LM_2(\rho))\end{bmatrix}}_{M_a(\rho)}\xi$$

$$\underbrace{\begin{bmatrix}e_z\\ z_\infty\\ e_f\end{bmatrix}}_{w} = \underbrace{\begin{bmatrix}I & 0 & 0\\ 0 & C_\infty & 0\\ 0 & 0 & -A_f^{-1}A_{212}\end{bmatrix}}_{C_a}\begin{bmatrix}e_z\\ x_c\\ \tilde{e}_1\end{bmatrix} \tag{57}$$

Box I.

Combining (51), (53) and (56), the LPV system capturing the dynamics between the external disturbance ξ and the performance measure $w = \mathrm{col}(e_z, z_\infty, e_f)$ is obtained as in (57), given in Box I, where $A_0(\rho) = A_c(\rho) + B_cK_0(\rho)C_c$.

The integrated LPV static feedback control and fault estimation design problem is formulated as:

Problem 3.1. Find a parameter-dependent feedback gain $\Delta(\rho)$ (and hence from (54) the feedback matrix $K(\rho)$) and a fixed observer gain matrix L (simultaneously) to minimize the $\mathcal{L}_2$ gain between ξ and w.

Define the matrix set

$$\mathcal{P} = \big\{X \in \mathbb{S}^+_{2m+3n-p+q} \ : \ X = \mathrm{diag}(X_1, X_1, X_2), \\ X_1 \in \mathbb{S}^+_{m+n},\ X_2 \in \mathbb{S}^+_{n-p+q}\big\} \tag{58}$$

and consider the optimization problem

Minimize γ with respect to $\Delta(\rho)$, L and $P_a \in \mathcal{P}$, subject to

$$\begin{bmatrix}P_aA_a(\rho)+A_a(\rho)^TP_a & P_aM_a(\rho) & C_a^T\\ * & -\gamma I & 0\\ * & * & -\gamma I\end{bmatrix} < 0, \qquad P_a > 0 \tag{59}$$

where the system matrices $A_a(\rho)$, $M_a(\rho)$ and C_a are defined in (57).

Remark 3.1. From the BRL, inequalities (59) implies $\|w\|_2 \leq \gamma\|\xi\|_2$. Thus, solving the optimization problem in (59) provides a sub-optimal solution to Problem 3.1.

Remark 3.2. Because of the specific structure imposed on P_a which is caused by assuming it belongs to the set $\mathcal{P}$ in (58), some conservatism is imposed and γ will only represent an upper bound on the true $\mathcal{L}_2$ gain between w and ξ. Note that defining P_a as a more generic structure will reduce the design conservatism but will increase the design complexity since the observer and controller gains, in terms of decision variables, are no longer decoupled. This represents a trade-off which always exists in this sort of formulation (e.g. see for example in Haddad and Bernstein (1993)).

The structure of $A_a(\rho)$ in (57) (since in particular it depends on $\Delta(\rho)$) implies that the matrix inequality in (59) is bilinear and the optimization problem in (59) becomes non-convex NP hard. To make progress, an iterative approach will be adopted to solve this problem.

Remark 3.3. An iterative approach, compared to a 'one-step' based method, is less attractive. However, again, there exists a trade-off between a 'one step' method and an iterative method in terms of designing LPV systems. In order to solve LPV/BMIs in one step, the so-called 'change of controller variable' method (Scherer, Gahinet, & Chilali, 1997) could be used to reformulate LPV/BMIs as LPV/LMIs, but this requires static feedback gains to be replaced by a higher order dynamic feedback controller. Furthermore, the 'change of the controller variable' method requires extra matrix equalities to be satisfied in the one step process.

Define another matrix set $\bar{\mathcal{P}} \subset \mathcal{P}$ according to

$$\bar{\mathcal{P}} = \big\{\bar{X} \in \mathbb{S}^+_{2m+3n-p+q} \ : \ \bar{X} = \mathrm{diag}(X_3, X_4, X_3, X_4, X_5), \\ X_3 \in \mathbb{S}^+_n,\ X_4 \in \mathbb{S}^+_m,\ X_5 \in \mathbb{S}^+_{n-p+q}\big\} \tag{60}$$

then the following lemma is critical to what follows:

Lemma 3.1. *Suppose $\Delta(\rho)$, L, γ and $P_a \in \mathcal{P}$ satisfy (59). Then there exists a change of coordinates $x \mapsto \bar{T}x = \bar{x}$ for the system in (57), where $\bar{T} = \mathrm{diag}(T, T, I_{n+q-p})$ where $T \in \mathbb{R}^{(n+m)\times(n+m)}$ and is nonsingular, so that in the new coordinates $(A_a(\rho), M_a(\rho), C_a) \mapsto (\bar{A}_a(\rho), \bar{M}_a(\rho), \bar{C}_a)$ the associated BRL matrix inequality*

$$\begin{bmatrix}\bar{P}_a\bar{A}_a(\rho)+\bar{A}_a(\rho)^T\bar{P}_a & \bar{P}_a\bar{M}_a(\rho) & \bar{C}_a^T\\ * & -\gamma I & 0\\ * & * & -\gamma I\end{bmatrix} < 0, \qquad \bar{P}_a > 0 \tag{61}$$

has a solution where $\bar{P}_a \in \bar{\mathcal{P}}$. In (61), $\bar{A}_a(\rho) = \bar{T}A_a(\rho)\bar{T}^{-1}$, $\bar{M}_a(\rho) = \bar{T}M_a(\rho)$, $\bar{C}_a = C_a\bar{T}^{-1}$. Furthermore, it is possible to choose T and hence $\bar{T}$ so that and $\bar{P}_a = \mathrm{diag}(\bar{P}_1, \bar{P}_2, \bar{P}_1, \bar{P}_2, P_e)$ and $\bar{B}_c = TB_c = B_c$.

Proof. Suppose the $P_a \in \mathcal{P}$ satisfying the BRL inequality in (59) is written as $P_a = \mathrm{diag}(P, P, P_e)$ where $P_e \in \mathbb{S}^+_{n-p+q}$ as defined in (58) and

$$P = \begin{bmatrix}P_{11} & P_{12}\\ P_{12}^T & P_{22}\end{bmatrix} \tag{62}$$

and $P_{22} \in \mathbb{S}^+_m$. Then consider the change of coordinates $x \mapsto \bar{T}\bar{x} = \bar{x}$ where

$$\bar{T} = \begin{bmatrix}T & 0 & 0\\ 0 & T & 0\\ 0 & 0 & I\end{bmatrix} \quad \text{and} \quad T = \begin{bmatrix}I & 0\\ P_{22}^{-1}P_{12}^T & I\end{bmatrix} \tag{63}$$

Let $\bar{A}_0(\rho) = TA_0(\rho)T^{-1}$ and $\bar{M}_c(\rho) = TM_c(\rho)$. Then define

$$\bar{P} = (T^{-1})^TPT^{-1} = \begin{bmatrix}\bar{P}_1 & 0\\ 0 & \bar{P}_2\end{bmatrix} = \begin{bmatrix}P_{11}-P_{12}P_{22}^{-1}P_{12}^T & 0\\ 0 & P_{22}\end{bmatrix} \tag{64}$$

since P is s.p.d. it follows from the Schur complement that $P_{11} - P_{12}P_{22}^{-1}P_{12}^T$ is also s.p.d. Let $\bar{P}_a = (\bar{T}^{-1})^T P_a \bar{T}^{-1}$ then it follows the matrix $\bar{P}_a = \text{diag}(\bar{P}, \bar{P}, P_e)$ and $\bar{P}_a \in \bar{\mathcal{P}}$ from the structure of $\bar{P}$ in (64).

Multiplying (59) on the left by $\text{diag}(\bar{T}^{-1}, I, I)^T$ and on the right by $\text{diag}(\bar{T}^{-1}, I, I)$ and using the fact $(T^{-1})^T P = \bar{P}T$ it follows (59) is satisfied if and only if (61) is satisfied. Consequently $\bar{P}_a$, $\Delta(\rho)$ and L is a solution to (61). Furthermore, using the structure of T in (63) and the structure of B_c in (4), in the new coordinates $TB_c = B_c$. □

Remark 3.4. Note that in (61)

$$\bar{P}_a\bar{A}_a(\rho) = \begin{bmatrix} \bar{P}\bar{A}_0(\rho) & \bar{P}\bar{B}_c\Delta(\rho)C_cT^{-1} & 0 \\ 0 & \bar{P}\bar{A}_0(\rho) + \bar{P}\bar{B}_c\Delta(\rho)C_cT^{-1} & -\bar{P}\bar{B}_c(K_0(\rho)+\Delta(\rho))C_0 \\ 0 & 0 & P_e(A_{11}+LA_{21}) \end{bmatrix} \tag{65}$$

where $\bar{A}_0(\rho) = TA_0(\rho)T^{-1}$ and

$$\bar{P}\bar{B}_c\Delta(\rho) = \begin{bmatrix} 0 \\ P_{22}B_u\Delta(\rho) \end{bmatrix} \tag{66}$$

Consequently defining $X(\rho) = P_{22}B_u\Delta(\rho)$ and $Y = P_eL$ renders (65) affine w.r.t. the decision variables $\bar{P}$, P_e, $X(\rho)$ and Y. This is crucial to the algorithm which follows.

Define

$$A_a(\rho)^{(j)} = \begin{bmatrix} A_0(\rho) & B_c(\sum_{i=1}^{j-1}\bar{\Delta}(\rho)^{(i)} + \bar{\Delta}(\rho)^{(j)})C_c & 0 \\ 0 & A_0(\rho) + B_c(\sum_{i=1}^{j-1}\bar{\Delta}(\rho)^{(i)} + \bar{\Delta}(\rho)^{(j)})C_c & -B_c(K_0(\rho) + \sum_{i=1}^{j-1}\bar{\Delta}(\rho)^{(i)} + \bar{\Delta}(\rho)^{(j)})C_0 \\ 0 & 0 & A_{11}(\rho) + L^{(j)}A_{21}(\rho) \end{bmatrix} \tag{67}$$

$$M_a(\rho)^{(j)} = \begin{bmatrix} 0 \\ \bar{M}_c(\rho) \\ -(M_1(\rho) + L^{(j)}M_2(\rho)) \end{bmatrix} \tag{68}$$

Note that in (67), $\Delta(\rho)$ has been decomposed as $\Delta(\rho) := \sum_{i=1}^{j-1}\bar{\Delta}(\rho)^{(i)} + \bar{\Delta}(\rho)^{(j)}$. During the iteration process, the first component $\sum_{i=1}^{j-1}\bar{\Delta}(\rho)^{(i)}$, calculated from the previous iterations, is treated as a known parameter in the current iteration. This component is used to update the initial value of the controller (i.e. $K_0(\rho) + \sum_{i=1}^{j-1}\bar{\Delta}(\rho)^{(i)}$) whilst the component $\bar{\Delta}(\rho)^{(j)}$ is the decision variable to be calculated in the current iteration. Now consider the iterative LMI based algorithm:

Algorithm 3.1.

Step 0. Set $j = 1$ and select the stopping criteria $\epsilon > 0$.

Step 1. Solve the LMI problem:

Minimize γ with respect to the decision variables $L^{(j)}$ and $P_a^{(j)} \in \mathcal{P}$ subject to

$$\begin{bmatrix} P_a^{(j)}A_a(\rho)^{(j)} + A_a^T(\rho)^{(j)}P_a^{(j)} & P_a^{(j)}M_a(\rho)^{(j)} & C_a^T \\ * & -\gamma I & 0 \\ * & * & -\gamma I \end{bmatrix} < 0 \qquad P_a^{(j)} > 0 \tag{69}$$

where $A_a(\rho)^{(j)}$ and $M_a(\rho)^{(j)}$ are defined in (67) and (68), and in the expression for $A_a(\rho)^{(j)}$, $\bar{\Delta}(\rho)^{(j)} = 0$. Since $P_a^{(j)} \in \mathcal{P}$ write $P_a^{(j)} = \text{diag}(P^{(j)}, P^{(j)}, P_e^{(j)})$ where $P_e^{(j)} \in \mathbb{S}^+_{n-p+q}$. Then defining $Y = P_e^{(j)}L^{(j)}$, inequality (69) is affine with respect to the variables $P^{(j)}$, $P_e^{(j)}$, Y and γ and constitutes an LMI optimization problem.

Let $\gamma^{(j)}$ be the optimal value of γ obtained from this optimization.

Step 2. Using the Lyapunov matrix $P^{(j)}$ from Step 1 and using the result of Lemma 3.1, create the change of coordinates matrix $\bar{T}^{(j)}$ exploiting the Lyapunov matrix $P_a^{(j)}$ from Step 1 and the fact that it belongs to $\mathcal{P}$.

In the new coordinates, $(A_a(\rho)^{(j)}, C_a, M_a(\rho)^{(j)}) \mapsto (\bar{A}_a(\rho)^{(j)}, \bar{C}_a, \bar{M}_a(\rho)^{(j)})$. Then using the arguments used to prove Lemma 3.1 and the ramifications discussed in Remark 3.4, the BRL inequality in the new coordinates becomes

$$\begin{bmatrix} \bar{P}_a^{(j)}\bar{A}_a(\rho)^{(j)} + \bar{A}_a^T(\rho)^{(j)}\bar{P}_a^{(j)} & \bar{P}_a^{(j)}\bar{M}_a(\rho)^{(j)} & \bar{C}_a^T \\ * & -\bar{\gamma} I & 0 \\ * & * & -\bar{\gamma} I \end{bmatrix} < 0 \qquad \bar{P}_a^{(j)} > 0 \tag{70}$$

Furthermore (70) has a feasible solution $\bar{P}^{(j)} = ((\bar{T}^{(j)})^{-1})^T P^{(j)} (\bar{T}^{(j)})^{-1} \in \bar{\mathcal{P}}$, $\bar{\Delta}(\rho)^{(j)} = 0$ and $\bar{\gamma} = \gamma^{(j)}$.

Now within this step solve the convex optimization problem

Minimize $\bar{\gamma}$ with respect to the decision variable $L^{(j)}$, $\bar{\Delta}(\rho)^{(j)}$ where $\bar{P}_a^{(j)} \in \bar{\mathcal{P}}$ subject to (70).

Using the arguments in the proof of Lemma 3.1 if $\bar{P}_a^{(j)}$ is written as $\bar{P}_a^{(j)} = \text{diag}(P_1^{(j)}, P_2^{(j)}, P_1^{(j)}, P_2^{(j)}, P_e^{(j)})$ and defining $X(\rho)^{(j)} = P_2^{(j)}B_u\bar{\Delta}(\rho)^{(j)}$ and $Y = P_e^{(j)}L^{(j)}$ then (70) is affine with respect to the decision variables $P_1^{(j)}, P_2^{(j)}, P_e^{(j)}, X(\rho)^{(j)}$ and Y. Let the optimal value of $\bar{\gamma}$ in (70) be written $\bar{\gamma}^{(j)}$. Since (70) has a feasible solution in which $\bar{\Delta}(\rho)^{(j)} = 0$, the solution to the optimization guarantees $\bar{\gamma}^{(j)} \leq \gamma^{(j)}$.

Step 3. Define $\bar{\Delta}(\rho)^{(j)} = (P_2^{(j)})^{-1}B_u^{-1}X(\rho)^{(j)}$.

Step 4. If $|\bar{\gamma}^{(j)} - \gamma^{(j)}| < \epsilon$ then stop the iteration and a *local* optimal feasible solution for $K(\rho)$ and L is given by

$$K(\rho) = K_0(\rho) + \sum_{i=1}^{j}\bar{\Delta}(\rho)^{(i)} \quad L = L^{(j)} \tag{71}$$

Otherwise update $j \to j+1$ and go to Step 1. □

Theorem 3.1. *The $\mathcal{L}_2$ gain bounds $\gamma^{(j)}$ arising from Algorithm 3.1, associated with the system in (59), converge to a local minimal $\gamma^\star$ with respect to the decision variables $\Delta(\rho)$, L and P_a.*

Proof. Algorithm 3.1, by construction, creates a series of scalars $\gamma^{(j)} \geq 0$ which all constitute upper bounds on the $\mathcal{L}_2$ gain of the system in (59). The key point to note (in Step 2) is that, by

construction $\gamma^{(j+1)} \leq \gamma^{(j)}$. Using the fact that $\{\gamma^{(j)}\}_{j=1}^{\infty}$ is bounded from below (since $\gamma^{(j)} \geq 0$ for all j), let $\gamma^\star$ be the greatest lower bound (glb) of $\{\gamma^{(j)}\}_{j=1}^{\infty}$ (Rudin, 1976). As in Theorem 3.14 from Rudin (1976), by definition

$$\gamma^{(j)} \geq \gamma^\star \quad (j = 1, 2, 3, \ldots) \tag{72}$$

However for every $\epsilon > 0$, there exists an integer N such that

$$\gamma^{(N)} < \gamma^\star + \epsilon \tag{73}$$

otherwise $\gamma^\star$ is not the glb of $\{\gamma^{(j)}\}_{j=1}^{\infty}$. Since $\{\gamma^{(j)}\}$ is non-increasing, for all $j \geq N$

$$\gamma^\star + \epsilon \geq \gamma^{(j)} \geq \gamma^\star - \epsilon \tag{74}$$

In other words, $\{\gamma^{(j)}\}_{j=1}^{\infty}$ converges to $\gamma^\star$. Consequently $\{\gamma^{(j)}\}_{j=1}^{\infty}$ is a Cauchy sequence (Rudin, 1976) and therefore for any $\epsilon > 0$ there exists an N_c such that for all $j > N_c$, $|\gamma^{(j+1)} - \gamma^{(j)}| < \epsilon$ and therefore the stopping criterion in Algorithm 3.1 is satisfied after a finite number of iterations, and an arbitrarily close approximation to the true local minima $\gamma^\star$ is found. □

Remark 3.5. Provided $K_0(\rho)$ is chosen so that $(A_c(\rho)+B_cK_0(\rho)C_c)$ is quadratically stable, Algorithm 3.1 will converge and yield the term $\Delta(\rho)$ to create the new controller gain $K(\rho) = K_0(\rho) + \Delta(\rho)$ (which constitutes the integrated controller design). Our argument is essentially, in the worst case, the algorithm will stop at the first iteration and return a value $\Delta(\rho) = 0$ and $\gamma = \gamma^{(1)}$ if it is unable to find a $\Delta(\rho)$ to reduce γ. However since the optimization problem which is solved using the algorithm is non-convex, different choices of $K_0(\rho)$ could lead to different (locally optimal) solutions.

The algorithm will now be demonstrated on a benchmark aircraft system from the RECONFIGURE project.

4. RECONFIGURE benchmark case study

The aim of the European FP7 funded RECONFIGURE project is to extend the automatic Guidance Navigation and Control (GNC) functions (within commercial civil aircraft) to make future flight tasks easier with a reduced pilot workload, and optimized aircraft performance. This can be translated into investigating and developing advanced aircraft GNC technologies that facilitate the automated handling of off-nominal and abnormal events. In this paper, the integrated scheme described in the earlier sections is employed to achieve and retain the required load factor[2] control performance in a RECONFIGURE benchmark problem involving the total loss of the angle of attack sensor. The proposed scheme will be evaluated *on the fully nonlinear RECONFIGURE benchmark* which includes a highly representative model of a generic AIRBUS civil commercial aircraft, detailed actuator and sensor models, as well as the angle of attack and speed protection components and measurement filters. The simulation model is 'invisible' for design purposes, and runs in a compiled fashion in a LINUX environment. The flight control computer component is extracted in a Simulink model which can be redesigned for FTC purposes (Goupil et al., 2014). *These represent one of the most detailed and sophisticated aircraft models Airbus use in the validation and verification cycle.*

In order to introduce a load factor tracking capability, integral action states are defined as

$$\dot{e}_I = n_z - r \tag{75}$$

[2] Load factor is the ratio of the lift of an aircraft to its weight and is unity at straight and level flight (Clancy, 1975). In the RECONFIGURE benchmark, load factor is the chosen 'controlled' variable.

Table 1
Mass and Centre Gravity cases (MC) definition[a].

MC reference	Gross weight (t)	Centre Gravity (CG) (%)
A	MFW	Max forward CG
B	MFW	Medium CG
C	MFW	Max aft CG
D	(MLW+MZFW)/2	Max forward CG
E	(MLW+MZFW)/2	Medium CG
F	(MLW+MZFW)/2	Max aft CG
G	(MTOW+MLW)/2	Max forward CG
H	(MTOW+MLW)/2	Medium CG
I	(MTOW+MLW)/2	Max aft CG

[a]In this table, 'MFW', 'MLW', 'MZFW' and 'MTOW' denote the maximum flight weight, the maximum landing weight, the maximum zero fuel weight and the maximum take-off weight, respectively. Note that in this table, numerical values cannot be provided explicitly due to industrial confidentiality restrictions.

where r is the reference load factor and n_z is the vertical load factor along the aircraft body z-axis. In this paper, the short period dynamics are used for the load factor control system design (Maciejowski, Hartley, & Siaulys, 2016; Puyou & Ezerzere, 2012), and the state variables are

$$x_p = \begin{bmatrix} e_I & q & \alpha \end{bmatrix}^T \tag{76}$$

where q is pitch rate and α denotes the angle of attack. Since the states x_p are measurable in the benchmark, in (1) $C_{p,1} = I$ and a full state feedback gain matrix is developed in this section. The system input vector and external disturbances are

$$u_p = \begin{bmatrix} \delta_{ie} & \delta_{oe} \end{bmatrix}^T \quad \xi = \begin{bmatrix} V_{vent} & \alpha_{vent} \end{bmatrix}^T \tag{77}$$

where δ_{ie} denotes an aggregation of the control deflections of the left and right inboard elevators and δ_{oe} denotes an aggregation of the control deflections of the left and right outboard elevators. For the RECONFIGURE benchmark (generic aircraft) model, both the inboard and outboard elevators are assumed to move in tandem. The external disturbance ξ contains variables V_{vent} and α_{vent} which denote the wind speed in an inertial reference system and the wind angle of attack. The system output vector and the controlled variable are

$$y_p = \begin{bmatrix} e_I & q & \alpha \end{bmatrix}^T, \quad z_\infty = e_I \tag{78}$$

In this paper, a total loss of angle of attack is assumed to occur from the beginning of the simulation and hence in (1) $H_p = [0 \;\; 0 \;\; 1]^T$. Three industrial validation activities (i.e. 'WIND-01', 'WIND-02' and 'WIND-03') were defined in RECONFIGURE to evaluate the efficacy of the scheme in the face of various wind profiles. The proposed scheme has been successfully validated in all three activities. However for brevity, only the activity 'WIND-01' is demonstrated in this paper. In 'WIND-01', the validation flight conditions are defined as:

- Auto-pilot and Auto-trust are engaged from the beginning of the simulation.
- Mach number M_a is 0.85 and altitude h is 41 000 ft.
- Landing gear and Slat/Flap parameters are in a 'clean' reconfiguration.
- The weight/balance cases are defined in Table 1.

In 'WIND-01', three wind profiles are involved: a headwind component W_x along the x axis (oriented forward); a rear wind component $-W_x$; and a lateral wind component W_y along the y axis. For each wind profile, nine flight conditions corresponding to Table 1 will be selected for robustness evaluation.

4.1. Design results on the fully nonlinear benchmark

For this paper, an LPV model has been created covering a wide part of the flight envelope to deal with the nonlinear benchmark

problem. The chosen scheduling parameters are

$$\rho = \begin{bmatrix} w\ (\text{tons}) & cg\ (\%) & V_c\ (\text{kt}) & M_a \end{bmatrix} \tag{79}$$

which represent the aircraft weight, the centre of gravity position, calibrated airspeed and Mach number. The scheduling parameters have been normalized in the interval [0 1], and all parameter-varying matrices are assumed to depend affinely on ρ, in particular $A(\rho) = A_0 + \sum_{i=1}^{4} \rho_i A_i$. In this paper, the matrix $A_f = I$. (The bandwidth of the associated filter is important and affects the robustness of the fault estimate: for a detailed discussion on the choice of A_f see page 216 in Alwi et al. (2011)). To approximate the dynamics of the inboard and outboard elevators in the nonlinear benchmark model, the transfer functions of two pre-filters in (3) are

$$f_{ie}(s) = \frac{1.0189}{0.1012s + 1} \quad f_{oe}(s) = \frac{1.012}{0.0910s + 1} \tag{80}$$

Here, using the LMI regional pole placement algorithm in Rotondo et al. (2014), the initial feedback gain is $K_0(\rho) = K_{0,0} + \sum_{i=1}^{4} \rho_i K_{0,i}$ where

$$K_{0,0} = \begin{bmatrix} 2.6008 & 3.0864 & 1.4263 & -1.9105 & -1.6145 \\ 3.5171 & 4.2307 & 2.0222 & -1.1417 & -1.2440 \end{bmatrix}$$

$$K_{0,1} = \begin{bmatrix} -0.1554 & -0.2725 & -0.0788 & 0.0323 & 0.0546 \\ -0.1601 & -0.2912 & -0.0585 & 0.0320 & 0.0550 \end{bmatrix}$$

$$K_{0,2} = \begin{bmatrix} -0.1115 & -0.1590 & 0.3531 & -0.0238 & -0.0126 \\ -0.1235 & -0.1657 & 0.4854 & -0.0411 & -0.0318 \end{bmatrix}$$

$$K_{0,3} = \begin{bmatrix} 0.2964 & 0.5094 & 0.1705 & -0.0627 & 0.0597 \\ 0.1761 & 0.3094 & 0.0052 & -0.3606 & -0.2559 \end{bmatrix}$$

$$K_{0,4} = \begin{bmatrix} 0.1085 & 0.3723 & 0.0078 & 0.1360 & 0.3732 \\ -0.1015 & 0.0303 & -0.2409 & -0.3283 & -0.1187 \end{bmatrix}$$

Implementing Algorithm 3.1, the improvement in terms of $\mathcal{H}_\infty$ performance γ is shown in Fig. 2. It is clear that γ keeps decreasing with increasing iteration number. After 80 iterations, the scheme stops and γ converges to 1.8233 and the resulting gain matrix $K(\rho) = K_0 + \sum_{i=1}^{4} \rho_i K_i$ where

$$K_0 = \begin{bmatrix} 1.8118 & 3.1674 & 0.8515 & -11.5541 & 5.2523 \\ 2.4913 & 3.8307 & 1.1172 & 6.6863 & -9.0291 \end{bmatrix}$$

$$K_1 = \begin{bmatrix} 0.4167 & -0.0888 & 0.2579 & 0.8956 & 0.3951 \\ 0.4469 & -0.0069 & 0.2887 & -2.8446 & 4.0360 \end{bmatrix}$$

$$K_2 = \begin{bmatrix} 0.1106 & 0.9803 & -0.4076 & -1.5442 & 0.5590 \\ 0.1607 & 1.5346 & -0.5279 & -7.7987 & 5.4862 \end{bmatrix}$$

$$K_3 = \begin{bmatrix} -0.3486 & 0.1032 & -0.2212 & 0.0206 & -1.6552 \\ -0.4240 & -0.2471 & -0.2811 & 4.5837 & -6.7296 \end{bmatrix}$$

$$K_4 = \begin{bmatrix} 0.1988 & 0.5048 & -0.2135 & -1.9292 & 2.7622 \\ 0.1983 & 0.1032 & -0.3140 & 1.1485 & -0.6753 \end{bmatrix}$$

The observer gain parameterization matrix L in (71) is given by

$$L = \begin{bmatrix} -1.4806 & 0.1847 & 0 \end{bmatrix} \tag{81}$$

4.2. Simulation results from 'WIND-01'

In this paper, the simulation results have been generated using the RECONFIGURE Functional Engineering Simulator (FES) (Fernandez et al., 2015) which is a software tool based on the MATLAB/SIMULINK modelling and simulation environment, specifically designed to support the industrial verification and benchmarking of the FDI/FTC algorithm prototypes designed by the partners in the RECONFIGURE project. The FES includes all the benchmark scenarios defined by AIRBUS for the evaluation of the FDI/FTC designs with traditional Monte Carlo analysis, and provides an interface for a worst-case search tool for implementing advanced optimization-based clearance methods (Goupil et al., 2015).

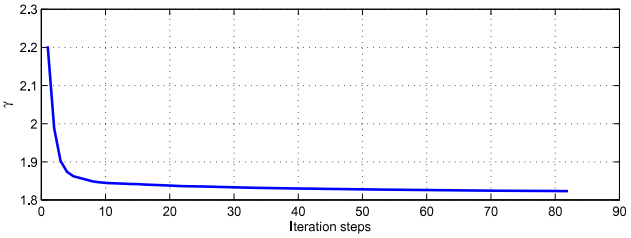

Fig. 2. Convergence of γ.

The idea here is to maintain the nominal desired load factor tracking of 1 despite total loss of angle of attack, as well as in the presence of wind (disturbance). As mentioned earlier, the results presented here are associated with an industrial evaluation using the FES for the so-called 'WIND-01' scenario. This involves three different wind directions (head, rear and side wind) as shown in Figs. 3, 4 and 5 respectively. For all the results that follow, a total loss of angle of attack measurements occurs from the start of the simulation. Note that the nominal trajectories of the states of the nonlinear benchmark are not shown explicitly due to industrial confidentiality restrictions. Instead, in the faulty cases, the difference between the fault affected system and the nominal one is shown.

Fig. 3 shows the results for the case of a headwind. Here, Fig. 3(a) shows the wind has a ramp profile which starts at 0 m/s and reaches a peak of 28.29 m/s (±55 kts) over an interval of 180 s. Each of the subplots in this figure (and subsequently Figs. 4 and 5) contains 9 different simulations at different points in the flight envelope as described in Table 1. The performance of the observer when estimating the fault in the angle of attack sensor and subsequently 'correcting' the faulty measurement (before it is sent to the controller) is shown in Fig. 3(f). The ideal signals are close to zero (i.e. close to nominal fault-free performance) which indicates that the corrected angle of attack measurement exactly matches the actual (fault-free) angle of attack of the aircraft. Fig. 3(f) shows small deviations at the beginning of the simulation when the fault occurs, which quickly reduce to zero, indicating good reconstruction performance from the observer despite the presence of the headwind. Fig. 3(b) shows that sliding is maintained despite the presence of the increasing wind. Fig. 3(e) shows that the controller manages to maintain the load factors close to the desired value of unity despite the existence of the wind profile and sensor faults. Finally, Figs. 3(c) and 3(d) show the inboard and outboard elevator demands sent to the actuators to maintain the load factor at its desired value in the presence of wind. A small 'spike' can be seen at the start of the simulations when the observer scheme is 'correcting' the faulty measurement, which quickly dissipate when the errors in Fig. 3(f) reduce close to zero.

The same evaluation as in the case for a headwind (at 9 different points in the flight envelope as described in Table 1) is now repeated for rear and side winds. The results are shown in Figs. 4 and 5. The rear and side wind profiles are shown in Figs. 4(a) and 5(a), and affect the aircraft from the tail and side respectively. Both have a ramp profile with magnitude of 28.29 m/s (±55 kts) during an interval of 180 s. As in the previous evaluation, Figs. 4(b) and 5(b) show that sliding still occurs as the $\|e_y\|$ are all close to zero despite the presence of wind and the total loss of angle of attack measurements from the beginning of the simulation. Figs. 4(e) and 5(e) show the errors between the estimated angle of

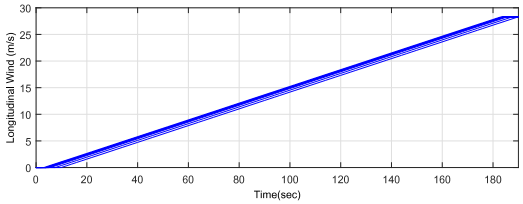

(a) Headwind component W_x

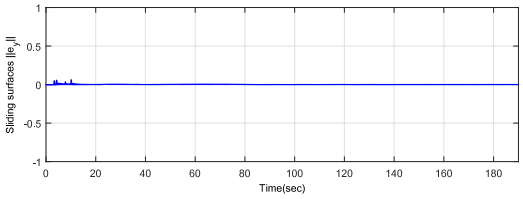

(b) Sliding surfaces $\|e_y\|$ in headwind profile

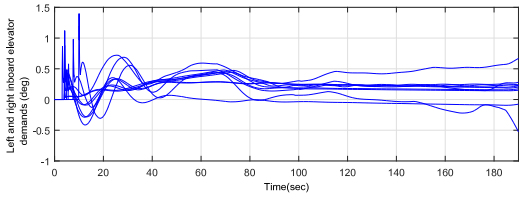

(c) Demands of inboard elevators in headwind profile

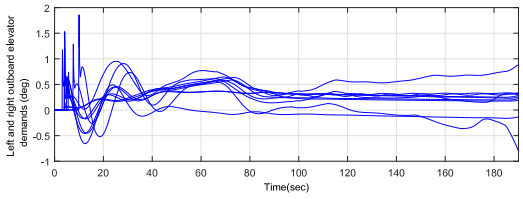

(d) Demands of outboard elevators in headwind profile

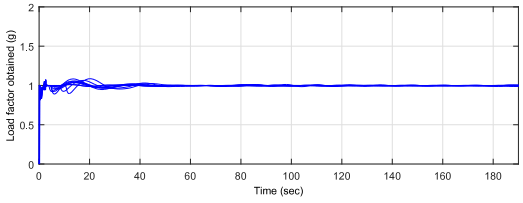

(e) Load factor obtained in headwind profile

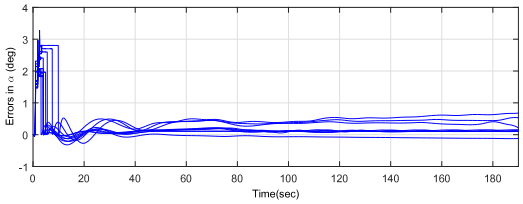

(f) Errors between the corrected and actual α in headwind profile

Fig. 3. Performance in headwind profile during 'WIND-01'.

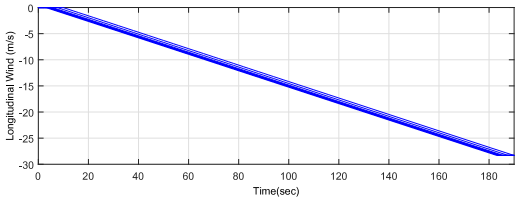

(a) Rear wind component $-W_x$

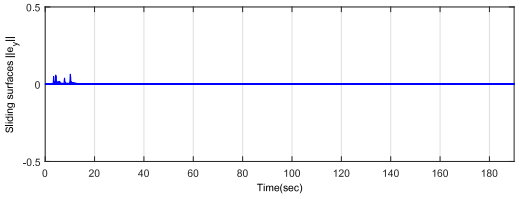

(b) Sliding surfaces $\|e_y\|$ in rear wind profile

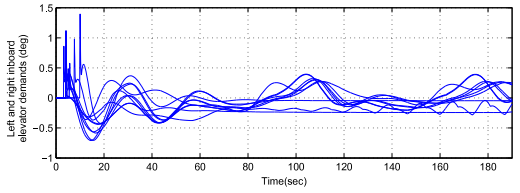

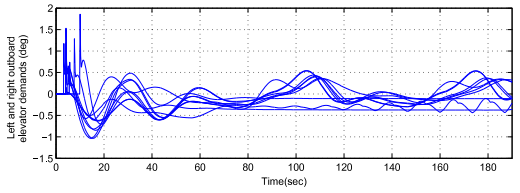

(c) Demands of inboard/outboard elevators in rear wind profile

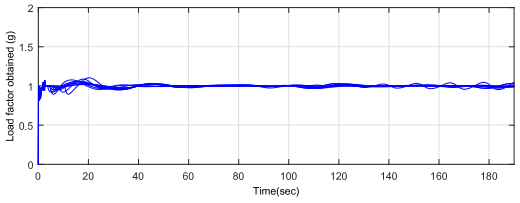

(d) Load factor obtained in rear wind profile

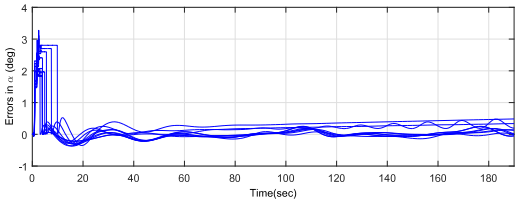

(e) Errors between the corrected and actual α in rear wind profile

Fig. 4. Performance in rear wind profile during 'WIND-01'.

attack and the actual angle of attack values. This clearly indicates that the sliding mode observer manages to reconstruct the faulty signals thus 'correcting' the faulty measurements (before they are used by the controller), despite the presence of the (unknown) wind. Again, this translates into good load factor performance as observed in Figs. 4(d) and 5(d), respectively, where all the load factors remain close to the desired value of unity despite the existence of the unknown wind profiles. The inboard and outboard elevator demands with respect to the head, rear and side wind profiles are depicted in Figs. 3(c), 3(d), 4(c) and 5(c), which reflect realistic control efforts in the presence of wind.

5. Conclusion

This paper has described the development of an integrated sensor fault tolerant control scheme, wherein the LPV sliding

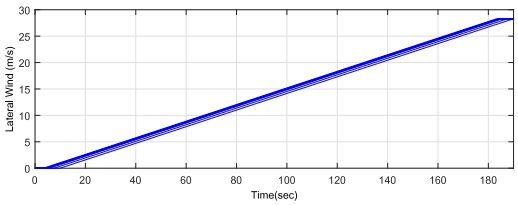

(a) Side wind component W_y

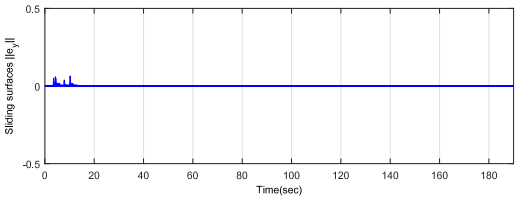

(b) Sliding surfaces $\|e_y\|$ in side wind profile

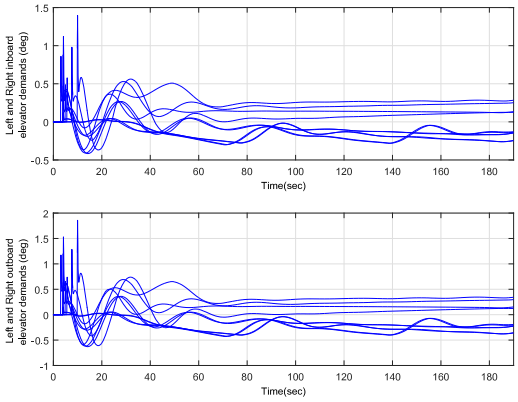

(c) Demands of inboard/outboard elevators in side wind profile

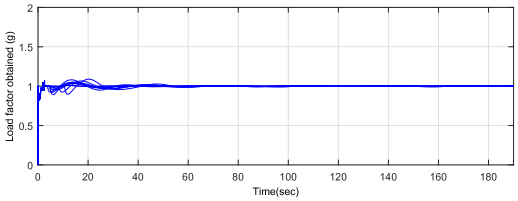

(d) Load factor obtained in side wind profile

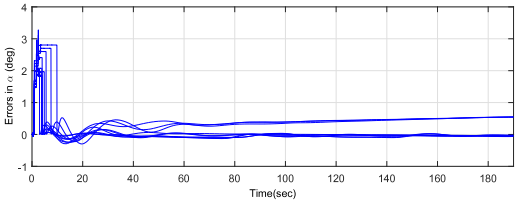

(e) Errors between the corrected and actual α in side wind profile

Fig. 5. Performance in side wind profile during 'WIND-01'.

mode observer and the LPV feedback controller gains are calculated simultaneously, which allows robust control performance and accurate fault estimation to be considered simultaneously. In this paper, the integrated design problem has been formulated as a LPV/BMI problem, and an iterative LMI based algorithm has been proposed to transform the non-convex LPV/BMI problem into a convex LPV/LMI problem which can be solved using a conventional LMI toolbox. The scheme has been applied to the fully nonlinear RECONFIGURE benchmark model. The results show good fault reconstructions in a scenario involving the total loss of angle of attack measurements, as well as maintenance of the desired load factor control performance over a wide range of the flight envelope in the presence of various wind profiles.

References

Alwi, H., & Edwards, C. (2008). Fault detection and fault-tolerant control of a civil aircraft using a sliding-mode-based scheme. *IEEE Transactions on Control Systems Technology*, *16*, 499–510.

Alwi, H., Edwards, C., & Marcos, A. (2012). Fault reconstruction using a LPV sliding mode observer for a class of LPV systems. *Journal of the Franklin Institute*, *349*, 510–530.

Alwi, H., Edwards, C., & Tan, C. P. (2011). *Fault detection and fault-tolerant control using sliding modes*. London: Springer.

Blanke, M., Kinnaert, M., Lunze, J., & Staroswiecki, M. (2016). Introduction to diagnosis and fault-tolerant control. In *Diagnosis and fault-tolerant control* (pp. 1–35). Berlin, Heidelberg: Springer Berlin Heidelberg.

Blondel, V. D., & Tsitsiklis, J. N. (1997). NP-hardness of some linear control design problem. *SIAM Journal on Control, Signals, Systems*, *35*.

Bokor, J., & Balas, G. (2004). Detection filter design for LPV systems-a geometric approach. *Automatica*, *40(3)*, 511–518.

Chandra, K. B., Alwi, H., & Edwards, C. (2017). Fault detection in uncertain LPV systems with imperfect scheduling parameter using sliding mode observers. *European Journal of Control*, *34*, 1–15.

Chen, L., Alwi, H., & Edwards, C. (2015). Integrated LPV controller/estimator scheme using sliding modes. In *Proceedings of the IEEE CDC* (pp. 5124–5129).

Chen, L., Edwards, C., & Alwi, H. (2015). LPV sliding mode observers for sensor fault reconstruction with erroneous scheduling parameter measurements. In *Proceedings of the IEEE CDC*. Osaka, Japan.

Chen, L., Edwards, C., & Alwi, H. (2017). On the synthesis of variable structure observers for LPV systems. In *Proceedings of the IEEE CDC* (pp. 5420–5425).

Chen, J., & Patton, R. J. (1999). *Robust model-based fault diagnosis for dynamic systems*. Norwell: Kluwer academic publishers.

Chen, L., Patton, R., & Goupil, P. (2016). Robust fault estimation using an LPV reference model: ADDSAFE benchmark case study. *Control Engineering Practice*, *49*, 194–203.

Chen, W. H., Yang, J., Guo, L., & Li, S. (2016). Disturbance-observer-based control and related methods – an overview. *IEEE Transactions on Industrial Electronics*, *63*, 1083–1095.

Clancy, L. J. (1975). *Aerodynamics*. London: Pitman Publishing Limited.

Davoodi, M. R., Meskin, N., & Khorasani, K. (2014). Integrated fault detection, isolation and control design for continuous-time Markovian jump systems with uncertain transition probabilities. In *Proceedings of the IEEE CDC* (pp. 5743–5749).

Ding, S. X. (2009). Integrated design of feedback controllers and fault detectors. *Annual Reviews in Control*, *33*, 124–135.

Edwards, C., Spurgeon, S. K., & Patton, R. J. (2000). Sliding mode observers for fault detection and isolation. *Automatica*, *36*, 541–553.

Efimov, D., Fridman, L., Raissi, T., Zolghadri, A., & Seydou, R. (2012). Interval estimation for LPV systems applying high order sliding mode techniques. *Automatica*, *48*, 2365–2371.

Fernandez, V., Montano, J., Marcos, A., Rosa, P., Kerr, M., & Dalbies, L. (2015). A tool for industrial verification and benchmarking of FDD/FTC designs. In *SAFEPROCESS'15* (pp. 1006–1011). Paris, France.

Gao, Z., & Ding, S. X. (2007). Actuator fault robust estimation and fault-tolerant control for a class of nonlinear descriptor systems. *Automatica*, *43*, 912–920.

Goupil, P., Boada-Bauxell, J., Marcos, A., Cortet, E., Kerr, M., & Costa, H. (2014). AIRBUS efforts toward advanced real-time fault diagnosis and fault tolerant control. In *19th IFAC world congress* (pp. 3741–3746). Cape Town, South Africa.

Goupil, P., Boada-Bauxell, J., Marcos, A., Rosa, P., Kerr, M., & Dalbies, L. (2015). An overview of the FP7 RECONFIGURE project: Industrial, scientific and technological objectives. In *SAFEPROCESS'15, Vol. 48* (pp. 976–981). Paris, France.

Haddad, W. M., & Bernstein, D. S. (1993). Explicit construction of quadratic lyapunov functions for the small gain, positivity, circle and popov theorems and their application to robust stability. *International Journal of Robust and Nonlinear Control*, *3*, 313–339.

Hecker, S., & Pififer, H. (2014). Affine LPV-modeling for the ADDSAFE benchmark. *Control Engineering Practice*, *31*, 126–134.

Ichalal, D., & Mammar, S. (2015). On unknown input observers for LPV systems. *IEEE Transactions on Industrial Electronics*, *62*, 5870–5880.

Jiang, B., Staroswiecki, M., & Cocquempot, V. (2006). Fault accommodation for nonlinear dynamic systems. *IEEE Transactions on Automatic Control*, *51*, 1578–1583.

Kabore, R., & Wang, H. (2001). Design of fault diagnosis filters and fault-tolerant control for a class of nonlinear systems. *IEEE Transactions on Automatic Control*, *46*, 1805–1810.

Khosrowjerdi, M., Nikoukhah, R., & Safari-Shad, N. (2004). A mixed H_2/H_∞ approach to simultaneous fault detection and control. *Automatica*, *40*, 261–267.
Kilsgaard, S., Rank, M. L., Niemann, H. H., & Stoustrup, J. (1996). Simultaneous design of controller and fault detector. In *Proceedings of the IEEE CDC* (pp. 628–629).
Kulcsr, B., Bokor, J., & Shinar, J. (2010). Unknown input reconstruction for LPV systems. *International Journal of Robust and Nonlinear Control*, *20*(5), 579–595.
Lan, J., & Patton, R. J. (2016). A new strategy for integration of fault estimation within fault-tolerant control. *Automatica*, *69*, 48–59.
Lan, J., & Patton, R. J. (2017a). Integrated design of fault-tolerant control for nonlinear systems based on fault estimation and T-S fuzzy modelling. *IEEE Transactions on Fuzzy Systems*, *25*(99), 1141–1154.
Lan, J., & Patton, R. J. (2017b). Integrated fault estimation and fault-tolerant control for uncertain lipschitz nonlinear systems. *International Journal of Robust and Nonlinear Control*, *27*, 761–780.
Levant, A. (1998). Robust exact differentiation via sliding mode technique. *Automatica*, *34*, 379–384.
de Loza, A. F., Bejarano, F. J., & Fridman, L. (2013). Unmatched uncertainties compensation based on high-order sliding mode observation. *International Journal of Robust and Nonlinear Control*, *23*, 754–764.
Maciejowski, J. M., Hartley, E. N., & Siaulys, K. (2016). A longitudinal flight control law to accommodate sensor loss in the reconfigure benchmark. *Annual Reviews of Control*, *42*, 212–223.
Marcos, A., & Balas, G. J. (2005a). A robust integrated controller/diagnosis aircraft application. *International Journal of Robust and Nonlinear Control*, *15*(12), 531–551.
Marcos, A., & Balas, G. J. (2005b). Nested integrated control and diagnostic filter design. In *IEEE conference on CDC-ECC*.
Mohammadpour, J., & Scherer, C. W. (2012). *Control of linear parameter varying systems with applications*. Springer.
Nett, C. T., Jacobson, C. A., & Miller, A. T. (1988). An integrated approach to controls and diagnostics: The 4-parameter controller. In *Proc. amer. contr. conf.* (pp. 824–835).
Niemann, H., & Stoustrup, J. (1997). Integration of control and fault detection: Nominal and robust design. In *SAFEPROCESS'97*, *Vol. 30* (pp. 331–336).
Pfifer, H., & Seiler, P. (2015). Robustness analysis of linear parameter varying systems using integral quadratic constraints. *International Journal of Robust and Nonlinear Control*, *25*, 2843–2864.
Puyou, G., & Ezerzere, P. (2012). Tolerance of aircraft longitudinal control to the loss of scheduling parameter information: toward a performance oriented approach. In *Proceeding of the 7th IFAC symposium on robust control design, Vol. 7* (pp. 393–399). Aalborg, Denmark.
Rodrigues, M., Hamdi, H., Braiek, N., & Theilliol, D. (2014). Observer-based fault tolerant control design for a class of LPV descriptor systems. *Journal of the Franklin Institute*, 3104–3125.
Rotondo, D., Nejjari, F., & Puig, V. (2014). Robust state-feedback control of uncertain LPV systems: An LMI-based approach. *Journal of the Franklin Institute*, *351*, 2781–2803.
Rudin, W. (1976). *Principles of mathematical analysis*. McGraw-Hill.
Sato, M., & Peaucelle, D. (2013). Gain-scheduled output-feedback controllers using inexact scheduling parameters for continuous-time LPV systems. *Automatica*, *49*, 1019–1025.
Scherer, C., Gahinet, P., & Chilali, M. (1997). Mulitobjective output-feedback control via LMI optimization. *IEEE Transactions on Automatic Control*.
Shamma, J. S. (2012). An overview of LPV systems. In *Control of linear parameter varying systems with applications* (pp. 3–26). Springer, Boston, MA.
Shtessel, Y., Edwards, C., Fridman, L., & Levant, A. (2013). *Sliding mode control and observation*. Basel: Springer.
Szaszi, I., Marcos, A., Balas, G. J., & Bokor, J. (2005). Linear parameter-varying detection filter design for a boeing 747-100/200 aircraft. *AIAA Journal of Guidance Control and Dynamics*, *28*, 461–470.
Utkin, V. (1992). *Sliding modes in control and optimization*. Heidelberg: Springer.
Wang, H., & Yang, G. H. (2009). Integrated fault detection and control for LPV systems. *International Journal of Robust and Nonlinear Control*, *19*, 341–363.
Weng, Z., Patton, R. J., & Cui, P. (2008). Integrated design of robust controller and fault estimator for linear parameter varying systems. In *17th IFAC world congress, Vol. 41* (pp. 4535–4539).
Wu, F. (1996). Induced $\mathcal{L}_2$ norm model reduction of polytopic uncertain linear systems. *Automatica*, *32*, 1417–1426.
Yang, H., Jiang, B., & Staroswiecki, M. (2009). Supervisory fault tolerant control for a class of uncertain nonlinear systems. *Automatica*, *45*, 2319–2324.
Zhang, Y., & Jiang, J. (2006). Issues on Integration of fault diagnosis and reconfigurable control in active fault-tolerant control systems. In *SAFEPROCESS'06, Vol. 39* (pp. 1437–1448).
Zhang, Y., & Jiang, J. (2008). Bibliographical review on reconfigurable fault-tolerant control systems. *Annual Reviews in Control*, *32*, 229–252.
Zhong, G. X., & Yang, G. H. (2015). Robust control and fault detection for continuous-time switched systems subject to a dwell time constraint. *International Journal of Robust and Nonlinear Control*, *25*, 3799–3817.
Zhou, K., & Doyle, J. (1998). *Essentials of robust control*. Prentice Hall.

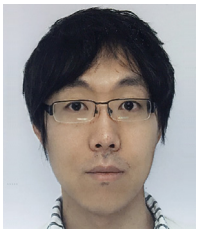

Lejun Chen was born in China. He received a Ph.D. degree in Electronics Engineering from the Intelligent System Group, Department of Electronics, the University of York. Since September 2013, he has been appointed to the position of Research Fellow at University of Exeter. His current research interests include model-based fault detection and fault tolerant control, and their applications to aerospace systems.

Halim Alwi was born in Malaysia. He studied at the University of Leicester and graduated in 2000 with a B.Eng. (Hons) in Mech. Engineering. From 2000 to 2004 he was an engineer at The NSTP (M) Bhd. In 2004 he moved back to the University of Leicester and was awarded a Ph.D. in 2008 in the area of fault tolerant control applied to aerospace systems. He is the co-author of over 60 refereed papers and two monographs on sliding mode control: 'Fault Detection and Fault Tolerant Control using Sliding Modes', Springer-Verlag (2011) and 'Fault Tolerant Control Scheme Using Integral Sliding Mode' Springer-Verlag (2016). He is currently a Senior Lecturer at the College of Engineering, Mathematics and Physical Sciences, University of Exeter.

Christopher Edwards is Professor of Control Engineering in the College of Engineering, Mathematics and Physical Sciences at the University of Exeter, UK. His current research interests are in sliding mode control and observation, and their application to fault detection and fault tolerant control problems. He is the author of over 400 refereed papers in these areas, and three books: *Sliding mode control: theory and applications* (1998), *Fault Detection and Fault Tolerant Control using Sliding Modes* (2011) and *Sliding Mode Control and Observation* (2014). In addition he co-edited the monograph *Fault Tolerant Flight Control: a Benchmark Challenge* (2010). His is currently chair of the IEEE technical committee on variable structure systems.